Polarization-Dependent Characteristics and Polarization Gating in Time-Resolved Optical Imaging of Skeletal Muscle Tissues

Chia-Wei Sun, Chih-Yu Wang, C. C. Yang, Yean-Woei Kiang, *Member, IEEE*, Chih-Wei Lu, I.-Jen Hsu, and Chii-Wann Lin

***Abstract*—The comparisons of the time-resolved transmitted intensity profiles and imaging results based on the polarization gating method between the samples of diluted milk, chicken breast tissue, and chopped chicken breast tissue revealed that the anisotropic structure of chicken breast tissue resulted in coherent coupling between the two inherent polarization directions and difficulty of using the polarization gating method for optical imaging through skeletal muscle tissues. To explore the polarization-dependent optical properties of chicken breast tissues, we calibrated the extinction coefficients of the polarization components parallel with and perpendicular to tissue filaments and the cross-polarized intensity-coupling coefficients between the two polarization components, based on the measured snake-photon intensity data. The calibrated values of these coefficients were quite consistent with previously reported. The extinction coefficient in the polarization along tissue filaments was significantly higher than that of the other polarization. Also, the cross-polarized coupling coefficient of the coupling from the polarization of tissue filaments into the other was stronger than that of inverse coupling.**

***Index Terms*—Diffuse photon, polarization gating, skeletal muscle tissue, snake photon, time-resolve imaging.**

I. Introduction

THERE HAS been an immediate need for developing more efficient tools for optically imaging human tissues with the aim at early diagnosis of abnormal cells. For thick tissues of several centimeters, ultrafast-optics techniques have been considered for optical imaging based on time gating of transmitted photons. In such a technique, picosecond or femtosecond pulses are applied to tissues, and the transmitted ballistic and snake photons are extracted with various time-gating methods, including Kerr gating [1], stimulated Raman scattering gating [2], sum-frequency generation gating [3], optical parametric amplification gating [4], and the use of a streak camera [5]. Because there is no clear boundary between weakly scattered snake photons and strongly scattered or multiply scattered diffuse photons in the transmitted time-resolved signals, careful design and implementation of the aforementioned time gating techniques are required. Since snake photons are quite few, particularly in thick tissues, other means have been developed, besides time gating, for improving signal-to-noise ratio [6]–[11]. Among them, polarization gating is an important method in optical imaging [7]–[11]. This method is based on the depolarization effect in random scattering of tissues. In other words, the input polarization state is lost in multiply scattered photons; however, it is partially preserved in weakly scattered photons. With linearly polarized input signals, the co-polarized transmitted photons would be more coherent and carry more information of tissue structures. The subtraction of the cross-polarized component from the co-polarized component, i.e., the removal of the incoherent part, has been shown to be a useful procedure for effective optical imaging. In this imaging process, the depolarization factor was usually calibrated from measured data for image construction. Nevertheless, such depolarization effect for discriminating between coherent and incoherent photons becomes less effective when there exists coherent coupling between two perpendicular polarization components. Such coherent coupling phenomena can particularly occur in tissues with anisotropic structures, such as skeletal muscle tissues [12]. In this situation, the conventional polarization gating method may become ineffective in optical imaging.

In this paper, we report our study results of anisotropic optical properties of skeletal muscle tissues. In experiments, chicken breast tissues were used as samples. Such a study is particularly important because phantoms, such as intralipid, milk, and other microparticle solutions are widely used for imitating the scattering and absorption of tissue structures. However, recently the differences of scattering characteristics between real tissues and phantoms caused much attention [13]. Here, we will report the time-gated imaging results of chicken breast tissues based on the polarization gating technique. Because such tissues consist of filaments with optically isotropic I bands (thin filament—containing actin) and anisotropic A bands (thick filament—containing myosin), e.g., [14], their optical transmission characteristics are quite different from other kinds of tissue and widely used phantoms. We compared the time-gated results between chicken breast tissue, chopped chicken breast tissue,

Manuscript received March 12, 2001; revised October 25, 2001. This work was supported in part by the National Health Research Institute, The Republic of China, under Grant NHRI-GT-EX89, and by the National Science Council, The Republic of China, under Grant NSC 89-2218-E-002-094 and Grant NSC 89-2218-E-002-095.

C.-W. Sun is with the Department of Electrical Engineering and Graduate Institute of Electro-Optical Engineering, National Taiwan University, Taipei, Taiwan, R.O.C.

C.-Y. Wang is with the Department of Bioengineering, I-Shou University, Kaohsiung, Taiwan, R.O.C.

C. C. Yang, Y.-W. Kiang, C.-W. Lu and I.-J. Hsu are with the Department of Electrical Engineering, Graduate Institute of Electro-Optical Engineering, and Graduate Institute of Communication Engineering, National Taiwan University, Taipei, Taiwan, R.O.C. (e-mail: ccy@cc.ee.ntu.edu.tw).

C.-W. Lin is with the Graduate Institute of Bioengineering, National Taiwan University, Taipei, Taiwan, R.O.C.

Publisher Item Identifier S 1077-260X(01)11234-7.

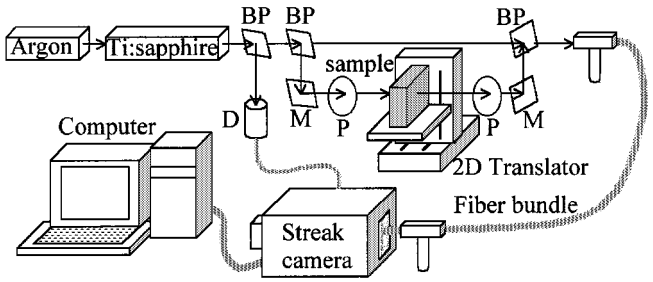

Fig. 1. Experimental setup. BP: beam splitter; P: polarizer; M: mirror; D: detector.

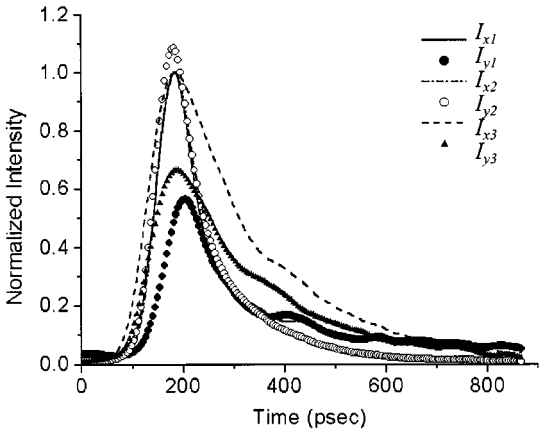

Fig. 2. Normalized and synchronized intensity profiles of the three samples. I_{xi} and I_{yi} represent the intensities of the polarization components parallel with and perpendicular to the input polarization direction, respectively, for sample i ($i = 1, 2$, and 3). Samples 1, 2, and 3 correspond to diluted milk, chicken breast tissue, and chopped chicken breast tissue, respectively. In the case of sample 2, the input polarization direction is along tissue filaments.

and diluted milk (phantom) for demonstrating the effects of coherent polarization coupling in skeletal muscle tissues. Then, in the second portion of this paper, we introduce a phenomenological model for describing the polarization-dependent optical characteristics of such a medium. We define the extinction coefficient of each linear polarization component and the polarization coupling coefficients for the cross-polarized interactions. We calibrate these coefficients based on the measurement data. The calibration results are quite reasonable when compared with what previously reported [15]. Physical interpretations of the results are also given.

The time-resolved imaging results with the polarization gating method are shown and discussed in Section II. Then, the calibration procedures, results, and their interpretations based on the phenomenological model are given in Section III. Finally, conclusions are drawn in Section IV.

II. Polarization-Gated Ultrafast-Optics Imaging in Skeletal Muscle Tissues

For optical imaging with polarization-gated snake photons, as shown in Fig. 1, an Argon laser pumped mode-locked Ti : sapphire laser was used to provide 76-MHz, around 100-fs laser pulses at 800 nm. The laser beam was split into three branches, one for triggering the used streak camera, the second one for propagating through samples, and the third one for temporal reference. About 200-mW average power was applied to the samples. Two polarizers, one before and the other after the samples, were used to control the input and output polarization for polarization gating. After the recombination of the sample and reference beams, signals were directed to the streak camera with a fiber bundle. The temporal resolution of the operation mode of the streak camera was 4.7 ps. The scanning mode was used in measurements, i.e., the fiber bundle end was always aligned with the incident laser beam while the samples were moved with a two-dimensional translation stage for image scanning. The scanning pixel size was 1 mm $\times$ 1 mm and the scanning area was 2 cm $\times$ 2 cm. For comparison, three different samples were prepared. They include diluted milk (sample 1), chicken breast tissue (sample 2), and chopped chicken breast tissue (sample 3). The diluted milk was contained in a plastic vessel with the transmission length of 10 cm. The chicken breast tissue sample has the thickness varying from 1.3 to 1.5 cm within the transverse scanning area. The transmission length of chopped chicken breast tissue was 1.4 cm. It was estimated that the dimension of chopped pieces was in the millimeter range.

Fig. 2 shows the time-resolved intensity profiles of three samples with the input linear polarization along the tissue filament direction (defined as the x direction) in the case of sample 2. To well align the polarization direction, we have carefully chosen the chicken breast tissue sample such that the filaments are almost the same along the sample thickness. For each sample, curves I_{xi} and I_{yi} ($i = 1, 2, 3$) represent the output polarization components parallel with (the x-axis) and perpendicular to (the y-axis) the filament orientation, respectively. The results shown in Fig. 2 were obtained by averaging over five pixels away from the regions of embedded objects (described below) in all the sample cases. For sample 2, the results were obtained from the pixels of the same sample thickness of about 1.5 cm. Also, all the intensity curves were normalized and synchronized such that the peaks of the three I_{xi} profiles had unity intensity and were located at the same time. With this procedure, one can still observe the relative shorter scattering tail in the sample 2 case, compared with the other two samples. This difference can be attributed to the organized tissue structures in skeletal muscle tissues. Such a structure was destroyed (at least partly) in the case of chopped chicken tissue. In this case, random scattering became stronger such that the intensity peak was delayed and the scattering tail was elongated.

In Fig. 2, the relative intensity and temporal peak position between I_{xi} and I_{yi} of the same sample provide us important information. In the case of diluted milk, I_{y1} (filled circles) is clearly lower than I_{x1} (continuous line). Also, the peak of I_{y1} profile is delayed with respect to that of I_{x1} profile. These observations represent the typical results of isotropic scattering, in which diffuse photons are equally distributed in the two mutually perpendicular polarization directions after strong scattering. In this situation, the subtraction of I_{y1} from I_{x1} results in coherent photons for effective imaging. Fig. 3(a) and (b) show such an example. Here, two pieces of lean pork (2 and 1 mm in thickness, respectively) as objects were placed within the diluted milk for imaging. Fig. 3(a) shows the image of integrated intensity with appropriate time gating of I_{x1}. Fig. 3(b) shows the image of time-gated I_{x1}–I_{y1}. Although I_{x1} can show the loca-

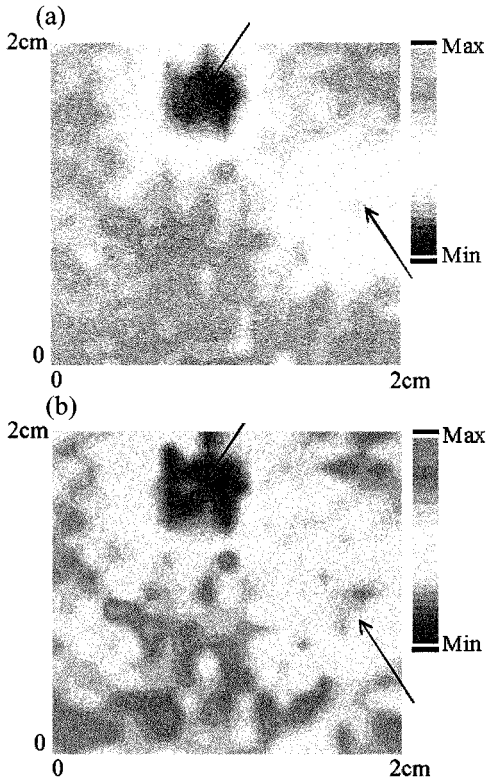

Fig. 3. Time-gated images of two pieces of lean pork in diluted milk with (a) I_{x1} and (b) I_{x1}–I_{y1}.

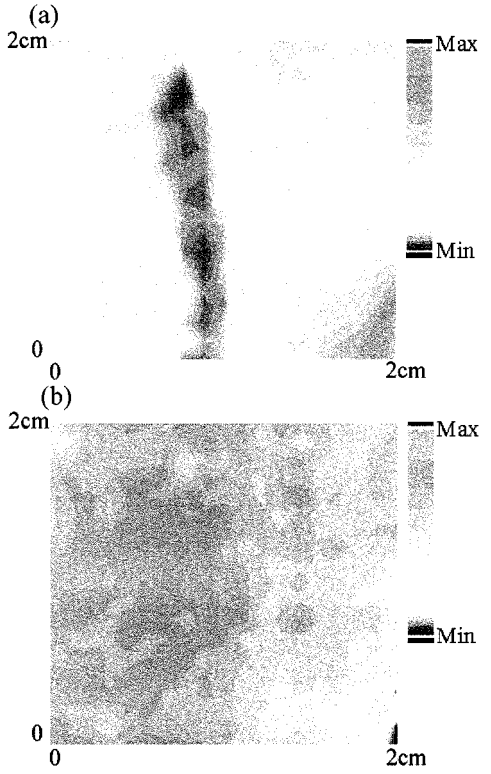

Fig. 4. Time-gated images of a chicken bone in chicken breast tissue with (a) I_{x2} and (b) I_{x2}–I_{y2}.

tions (red spots) of the two pieces of pork, I_{x1}–I_{y1} does provide a clearer image, particularly for the smaller and thinner piece on the right.

In the case of chicken breast tissue (sample 2), the intensity profiles in Fig. 2 show that I_{y2} (empty circles) is slightly higher than I_{x2} (dash-dotted line—close to the continuous line). This indicates that besides possible random scattering in such a medium, coherent coupling between the two polarization components occurs due to the organized structure of the tissue. Due to certain coherent cross-polarized interactions, signal polarization seemed to rotate such that I_{y2} became higher than I_{x2} at the output. In this situation, both I_{x2} and I_{y2} were quite coherent, particularly before and near their peaks. Hence, the conventional polarization gating technique, i.e., imaging with I_{x2}–I_{y2}, became difficult. Fig. 4(a) and (b) show the imaging results with a thin chicken bone of diameter 1–2 mm (as the object) sticking into the breast tissue sample. Parts (a) and (b) show the images of I_{x2} and I_{x2}–I_{y2}, respectively. The result of I_{x2} provides a rough picture of the chicken bone; however, I_{x2}–I_{y2} leads to no feature at all. The imaging results confirm the coherent polarization evolution besides random scattering in skeletal muscle tissues.

To further explore the case of chicken tissue sample, we also conducted the similar measurements with the input linear polarization perpendicular to the filament orientation, i.e., y-axis. The corresponding time-resolved intensity profiles of the two input polarization directions, i.e., I_{xi} and I_{yi} ($i = x$ and y, representing the input polarization along the x and y axes, respectively), are plotted in Fig. 5. Again, these profiles were obtained by averaging the measurement results of five pixels in the regions of 1.5 cm in sample thickness and away from the stuck chicken bone. In the case of the x-(y-) input polarization, the intensity profiles were normalized and synchronized with respect to the peak of the I_{xx} (I_{yy}) profile. Note that I_{xx} and I_{yx} in Fig. 5 are identical to I_{x2} and I_{y2} in Fig. 2, respectively. In Fig. 5, one can see the good coincidence of the I_{xx} and I_{yy} profiles (continuous and dash-dotted lines, respectively), indicating the similar scattering characteristics. The difference between the I_{yx} and I_{xy} profiles (filled symbols and empty symbols, respectively), particularly their different heights, shows different polarization coupling effects between the two input polarization directions. Fig. 6 shows similar results to Fig. 5, except that the data were taken in the region of the stuck chicken bone. In this region, the chicken tissue thickness was also 1.5 cm. Therefore, the comparison between Figs. 5 and 6 reveals the effect of chicken bone scattering. The comparison shows that the cross-polarized energy transfer has been reduced in either input polarization case. This change can be attributed to the more isotropic scattering of the chicken bone that weakens the coherent energy transfer between the two polarization components. The other observation is that the incoherent scattering, i.e., energy transfer into diffuse photons, becomes stronger due to the existence of the chicken bone. The effect of the chicken bone scattering will be further explored in the next section when we discuss the results of Table I.

Then, in the case of chopped tissue (sample 3), the chicken tissue was chopped and stirred to become statistically homogeneous. However, because the chopped pieces still had a dimension in the millimeter range, the basic tissue structures might still be partly preserved. In this situation, as shown in Fig. 2,

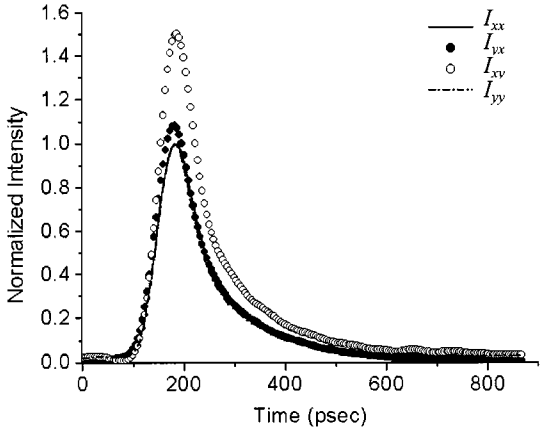

Fig. 5. Normalized and synchronized intensity profiles of the case of chicken breast tissue with two different input polarization directions. I_{xx} (I_{xy}) and I_{yx} (I_{yy}) represent the intensities of the polarization components parallel with and perpendicular to tissue filaments, respectively, when the input polarization is parallel with (perpendicular to) tissue filaments. The results were obtained at lateral positions of 1.5 cm in thickness away from the stuck chicken bone.

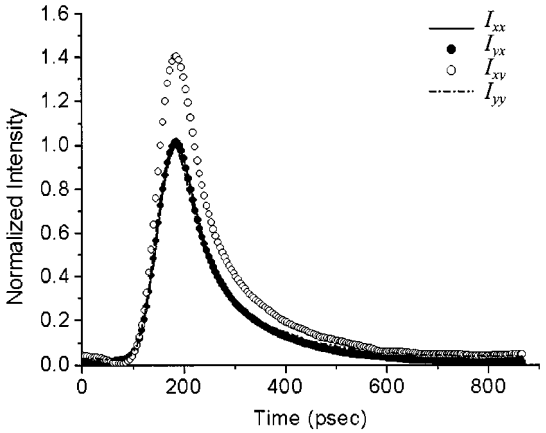

Fig. 6. Similar to Fig. 5, except that the results were obtained at lateral positions of 1.5 cm in thickness right at the location of the stuck chicken bone.

I_{x3} (short-dashed line) is significantly stronger than I_{y3} (filled triangles) with almost no time difference between their peaks. The relatively broader intensity profiles, compared to those of the chicken tissue case (I_{x2} and I_{y2}), indicate stronger random scattering, which transfers energy into diffuse photons. Fig. 7(a) and (b) show the images of I_{x3} and I_{x3}–I_{y3}, respectively, with the same chicken bone sticking into the chopped chicken tissue. The rough picture of the bone can be seen from I_{x3}. The configuration of the bone can also be seen from I_{x3}–I_{y3}. The results in Figs. 2 and 7 reveal the mixed effects of coherent polarization coupling and enhanced random scattering in chopped chicken tissue. Note that because the filament structure might not be completely destroyed in the chopped sample, Fig. 7(b) shows strong spatial variation in polarization difference imaging.

From the comparisons of the results between the three different samples, it is reasonable to hypothesize that in chicken breast tissues or skeletal muscle tissues, there exist coherent cross-polarized coupling mechanisms to control the relative intensity evolution of the polarization components. Such mechanisms may include the polarization rotation due to medium

TABLE I
FIVE SETS OF EXTINCTION AND COUPLING COEFFICIENTS (UNIT: cm^{-1})

	S1	S2	S3	S4	S5
μ_x	2.41-3.39	3.11-3.79	2.96-3.45	2.26-2.93	2.87-3.88
μ_y	1.43-2.5	1.92-2.53	1.46-2.13	1.37-1.89	2.32-3.3
κ_{xy}	0.49-0.51	0.78-0.8	0.95-1.01	0.65-0.67	0.76-0.82
κ_{yx}	1.61-1.69	2.79-2.82	2.57-2.72	1.69-1.86	2.14-2.27

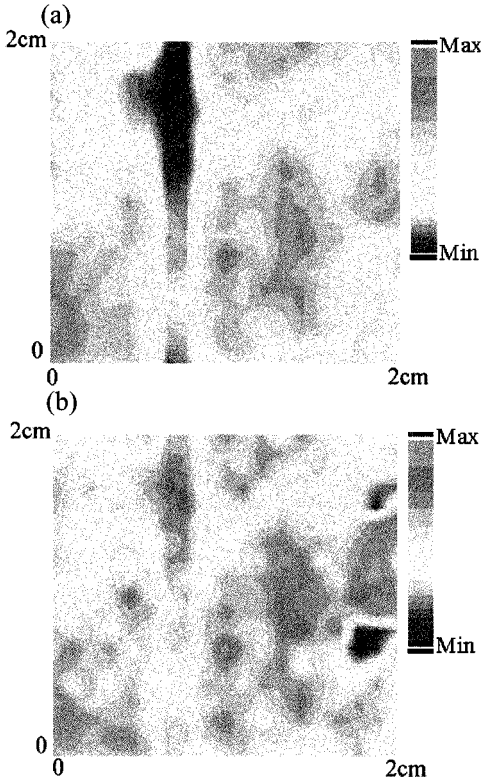

Fig. 7. Time-gated images of the chicken bone in chopped chicken breast tissue with (a) I_{x3} and (b) I_{x3}–I_{y3}.

birefringence, depolarization scattering, and polarization-dependent absorption. These mechanisms are partly destroyed after the tissues are chopped. With those mechanisms, the characteristics of snake photons in skeletal muscle tissues are quite different from those of random-scattering phantoms. Also, the conventional polarization-gating technique becomes less effective in skeletal muscle tissues.

III. POLARIZATION DEPENDENT CHARACTERISTICS OF SKELETAL MUSCLE TISSUES

As discussed in the last section, polarization-dependent snake-photon intensity in skeletal muscle tissues is controlled by several possible factors, including the optical birefringence, depolarization scattering, and polarization-sensitive loss mechanisms. The identification of each possible factor requires quite many efforts in research. In this section, we propose a phenomenological model to describe the variation of polarized snake-photon intensity. We collect all the cross-polarized interactions into lumped polarization coupling parameters. In this model, we express the evolution of the time-gated

optical intensities in the two inherent polarization directions, i.e., polarization along tissue filaments (the x direction) and the perpendicular component (the y direction), I'_x and I'_y, respectively, as

$$\frac{\partial I'_x}{\partial z} = -\mu_x I'_x + \kappa_{xy} I'_y \tag{1a}$$

$$\frac{\partial I'_y}{\partial z} = -\mu_y I'_y + \kappa_{yx} I'_x. \tag{1b}$$

Here, μ_x and μ_y stand for the extinction coefficients of the two inherent polarization components. Also, κ_{xy} and κ_{yx} represent the polarization coupling coefficients for power coupling from y-polarization into x-polarization and that from x-polarization into y-polarization, respectively. Here, signal propagation is assumed to be along the z direction. The solution forms of the coupled equations in (1a) and (1b) with initial conditions I'_{x0} and I'_{y0} can be written in a matrix form as shown in (2), at the bottom of the page. Here, λ_1 and λ_2 are the two roots of the characteristic equation for (1a) and (1b), given by

$$\lambda_1 = \tfrac{1}{2}\left[-(\mu_x+\mu_y) + \sqrt{(\mu_x-\mu_y)^2 + 4\kappa_{xy}\kappa_{yx}}\,\right] \tag{3a}$$

$$\lambda_2 = \tfrac{1}{2}\left[-(\mu_x+\mu_y) - \sqrt{(\mu_x-\mu_y)^2 + 4\kappa_{xy}\kappa_{yx}}\,\right]. \tag{3b}$$

Snake photon data were then used for calibrating the two extinction coefficients and two coupling coefficients. The snake photon data were obtained by time gating the time-resolved intensity profiles with duration of 50 ps from the leading edges of the profiles. Because the streak camera provided different gain factors for different levels of detected signals, calibration factors were carefully estimated for retrieving the signal optical intensities. The calibration procedures are as follows. We first choose five positions in the two-dimensional lateral scan of the chicken breast tissue. The tissue thickness at these five points could be different. The three sets of measurements of input polarization along the x and y axes, and 45° off either axis are used to provide six givens for solving the four-unknown problem in (2). Since we have givens more than unknowns and to obtain more accurate results, we adopted the method of least squares, as expressed by (4), shown at the bottom of the page. Here, the last subscript of I' means different data from different input polarization conditions. After we obtained the values of the four elements of the matrix on the left-hand side of (4), we solved numerically four nonlinear equations of μ_x, μ_y, κ_{xy}, and κ_{yx}. The set of nonlinear equations resulted in more than one set of solutions. However, only one set of solutions has all positive values and is in the reasonable ranges when compared with previously reported [15]. In estimating the aforementioned calibration factors, there existed certain uncertainties. It was found that with this factor varied by a factor of five, the calibrated results did not change significantly, as shown by the ranges in Table I.

Table I listed five sets of calibrated results, corresponding to five locations. Among them, sets S1 through S4 correspond to the locations away from the stuck chicken bone and set S5 corresponds to a location in the region of the bone. The tissue thickness of sets S1 through S5 are about 1.5, 1.5, 1.4, 1.3, and 1.5 cm, respectively. The ranges of values were obtained by varying the calibration factor within a reasonable range (by a factor of five). From the results, one can see that without the chicken bone, the extinction coefficient in the polarization direction of tissue filament ranges from 2.26 through 3.79 cm^{-1}. These values are consistent with the reported data of chicken breast tissues in this wavelength range [15]. It is interesting to find that the extinction coefficient along the other polarization direction, which ranges from 1.37 through 2.53 cm^{-1}, is relatively smaller by a significant amount. Such a difference can be attributed to the induction of polarization current by the incident ac electric field along tissue filaments. With the polarization current, dipole re-radiation and hence scattering are expected to be stronger in this polarization direction. It has been well studied in electromagnetic theories that a thin dielectric cylinder of infinite length results in a larger scattering cross section with incident linear polarization along the cylinder length, when compared with the other incident polarization, e.g., [16]. Although tissue

$$\begin{bmatrix} I'_x \\ I'_y \end{bmatrix} = \begin{bmatrix} (\lambda_2+\mu_x)e^{\lambda_1 z} - (\lambda_1+\mu_x)e^{\lambda_2 z} & \left(e^{\lambda_2 z} - e^{\lambda_1 z}\right)\kappa_{xy} \\ \dfrac{(\lambda_1+\mu_x)(\lambda_2+\mu_x)}{\kappa_{xy}}\left(e^{\lambda_1 z} - e^{\lambda_2 z}\right) & (\lambda_2+\mu_x)e^{\lambda_2 z} - (\lambda_1+\mu_x)e^{\lambda_1 z} \end{bmatrix} \bullet \frac{1}{\lambda_2-\lambda_1}\begin{bmatrix} I'_{x0} \\ I'_{y0} \end{bmatrix} \tag{2}$$

$$\frac{1}{\lambda_2-\lambda_1}\begin{bmatrix} (\lambda_2+\mu_x)e^{\lambda_1 z} - (\lambda_1+\mu_x)e^{\lambda_2 z} & \dfrac{(\lambda_1+\mu_x)(\lambda_2+\mu_x)}{\kappa_{xy}}\left(e^{\lambda_1 z} - e^{\lambda_2 z}\right) \\ \left(e^{\lambda_2 z} - e^{\lambda_1 z}\right)\kappa_{xy} & (\lambda_2+\mu_x)e^{\lambda_2 z} - (\lambda_1+\mu_x)e^{\lambda_1 z} \end{bmatrix}$$

$$= \left(\begin{bmatrix} I'_{x01} & \cdots & I'_{x0n} \\ I'_{y01} & \cdots & I'_{y0n} \end{bmatrix}\begin{bmatrix} I'_{x01} & I'_{y01} \\ \vdots & \vdots \\ I'_{x0n} & I'_{y0n} \end{bmatrix}\right)^{-1}\begin{bmatrix} I'_{x01} & \cdots & I'_{x0n} \\ I'_{y01} & \cdots & I'_{y0n} \end{bmatrix}\begin{bmatrix} I'_{x1} & I'_{y1} \\ \vdots & \vdots \\ I'_{xn} & I'_{yn} \end{bmatrix} \tag{4}$$

filaments cannot be exactly modeled as thin dielectric cylinders of infinite length, it is reasonable to expect stronger scattering and hence a larger extinction coefficient with the input polarization along tissue filaments.

Regarding the cross-polarized coupling coefficients, κ_{yx} (ranging from 1.61 through 2.82 cm^{-1}) is significantly larger than κ_{xy} (ranging from 0.49 through 1.01 cm^{-1}). It means that coupling from tissue filament polarization into the other polarization direction is significantly stronger than the coupling of the other way. This may again indicate that scattering in the polarization direction of tissue filaments is relatively stronger. The comparisons between the results of set S5 with other sets show clearly that the scattering in this region is more isotropic due to the existence of the chicken bone, as supported by the observation that the values of μ_x and μ_y in this region are closer. Note that the scattering includes two parts: scattering of coherent photons into the incoherent component (diffuse photons) of either polarization and scattering of coherent photons in one polarization into the coherent component of the other polarization. The large contrast between κ_{xy} and κ_{yx} in set S5, in spite of the small difference between μ_x and μ_y, can be attributed to the possibility that the major contribution of the chicken bone is to transfer energy into incoherent components (diffuse photons). This hypothesis is consistent with the comparison between Figs. 5 and 6, which shows that optical intensities are more intense at the tails in the region of the stuck chicken bone. The connection between the relative magnitude of the cross-polarized coupling coefficient and the relative contribution of coherent and incoherent scattering deserves further investigation.

IV. Conclusions

We have compared the time-resolved transmitted optical intensity profiles and imaging results of diluted milk, chicken breast tissue, and chopped chicken breast tissue based on the conventional polarization gating method of time-resolved imaging. The result in Fig. 3 implied that the polarization gating method was quite effective in imaging inhomogeneous objects in an isotropic turbid medium. Because chicken breast tissue had a deterministically anisotropic property, it led to coherent coupling between the two linear polarization components. The coherent coupling resulted in difficulty of using the conventional polarization gating method for optical imaging of skeletal muscle tissues. To explore the polarization-dependent optical properties of chicken breast tissues, we defined the extinction coefficients of the polarization components parallel with and perpendicular to tissue filaments and the cross-polarized intensity-coupling coefficients between the two polarization components. Based on the measured snake-photon intensity data of three different input polarization conditions, we have calibrated these coefficients. The values of the extinction coefficients were quite consistent with previously reported. Besides, we found that the extinction coefficient with polarization along tissue filaments was significantly higher than that of the other polarization. Also, the cross-polarized coupling coefficient of the coupling from the direction of tissue filaments into the other polarization was stronger than that of inverse coupling. Preliminary interpretations were given. Further understanding relies on future investigation.

References

[1] L. Wang, P. P. Ho, C. Liu, and R. R. Alfano, "Ballistic 2-D imaging through scattering walls using an ultrafast optical Kerr gate," *Science*, vol. 253, pp. 769–771, 1993.

[2] M. D. Duncan, R. Mahon, L. L. Tankersley, and J. Reintjes, "Time-gated imaging through scattering media using stimulated Raman amplification," *Opt. Lett.*, vol. 16, pp. 1868–1870, 1991.

[3] E. Abraham, E. Bordenave, N. Tsurumachi, G. Jonusauskas, J. Oberle, and C. Rulliere, "Real-time two-dimensional imaging in scattering media by use of a femtosecond Cr^{4+} : forsterite laser," *Opt. Lett.*, vol. 25, pp. 929–931, 2000.

[4] C. Doule, T. Lepine, P. Georges, and A. Brun, "Video rate depth-resolved two-dimensional imaging through turbid media by femtosecond parametric amplification," *Opt. Lett.*, vol. 25, pp. 353–355, 2000.

[5] K. M. Yoo, B. B. Das, and R. R. Alfano, "Imaging of a translucent object hidden in a highly scattering medium from the early portion of the diffuse component of a transmitted ultrafast laser pulse," *Opt. Lett.*, vol. 17, pp. 958–960, 1992.

[6] L. Wang, P. P. Ho, and R. R. Alfano, "Time-resolved Fourier spectrum and imaging in highly scattering media," *Appl. Opt.*, vol. 32, pp. 5043–5048, 1993.

[7] J. M. Schmitt, A. H. Gandjbakhche, and R. F. Bonner, "Use of polarized light to discriminate short-path photons in a multiply scattering medium," *Appl. Opt.*, vol. 31, pp. 6535–6546, 1992.

[8] H. Horinaka, K. Hashimoto, K. Wada, Y. Cho, and M. Osawa, "Extraction of qusai-straightforward-propagating photons from diffused light transmitting through a scattering medium by polarization modulation," *Opt. Lett.*, vol. 20, pp. 1501–1503, 1995.

[9] S. G. Demos and R. R. Alfano, "Temporal gating in highly scattering media by the degree of optical polarization," *Opt. Lett.*, vol. 21, pp. 161–163, 1996.

[10] S. P. Morgan, M. P. Khong, and M. G. Somekh, "Effects of polarization state and scatterer concentration on optical imaging through scattering media," *Appl. Opt.*, vol. 36, pp. 1560–1565, 1997.

[11] V. Sankaran, J. T. Walsh, Jr., and D. J. Maitland, "Polarized light propagation through tissue phantoms containing densely packed scatterers," *Opt. Lett.*, vol. 25, pp. 239–241, 2000.

[12] S. K. Gayen, M. E. Zevallos, M. Alrubaiee, J. M. Evans, and R. R. Alfano, "Two-dimensional near-infrared transillumination imaging of biomedical media with a chromium-doped forsterite laser," *Appl. Opt.*, vol. 37, pp. 5327–5336, 1998.

[13] V. Sankaran, M. J. Everett, D. J. Maitland, and J. T. Walsh, Jr., "Comparison of polarized-light propagation in biological tissue and phantoms," *Opt. Lett.*, vol. 24, pp. 1044–1046, 1999.

[14] A. J. Vander, J. H. Sherman, and D. S. Luciano, *Human Physiology, The Mechanisms of Body Function*, sixth ed. New York: McGraw-Hill, 1994, p. 304.

[15] G. Marquez, L. V. Wang, S. P. Lin, J. A. Schwartz, and S. L. Thomsen, "Anisotropy in the absorption and scattering spectra of chicken breast tissue," *Appl. Opt.*, vol. 37, pp. 798–804, 1998.

[16] G. T. Ruck, D. E. Barrick, W. D. Stuart, and C. K. Krichbaum, *Radar Cross Section Handbook*. New York: Plenum, 1970, vol. 4, p. 221.

Chia-Wei Sun was born in Taiwan, R.O.C., on September 27, 1975. He received the B.S. degree in electrical engineering from National Cheng Kung University, Tainan, Taiwan, in 1997 and the M.S. degree in biomedical engineering from National Yang-Ming University, Taipei, Taiwan, in 1999. He is currently working toward the Ph.D. degree at the Graduate Institute of Electro-Optical Engineering, National Taiwan University.

His research interests include biomedical photonics, optical imaging techniques, and fluorescence spectrum analysis.

Chih-Yu Wang, photograph and biography not available at the time of publication.

C. C. Yang was born in Cha-I, Taiwan, R.O.C., in 1954. He received the B.S. degree in electrical engineering from National Taiwan University, Taipei, in 1976, and the M.S. and Ph.D. degrees in electrical engineering from the University of Illinois at Urbana-Champaign in 1981 and 1984, respectively.

He then joined the Department of Electrical and Computer Engineering, The Pennsylvania State University, State College, as an Assistant Professor in 1984. He received his tenure and was promoted to Associate Professor in 1990. In 1993, he joined the Graduate Institute of Electro-Optical Engineering and the Department of Electrical Engineering, National Taiwan University, as a Professor. He has published more than 150 papers in technical journals and conferences. His research interests include ultrafast fiber and semiconductor optics, fabrication of fiber gratings and their applications, quantum-well intermixing and its applications, nonlinear optics, GaN-related materials and devices, and biophotonics.

Yean-Woei Kiang (S'81–M'84) was born in Panchiao, Taiwan, R.O.C., in 1954. He received the B.S.E.E., M.S.E.E., and Ph.D. degrees from the National Taiwan University, Taipei, Taiwan, in 1977, 1979, and 1984, respectively.

In 1979, he joined the faculty of the Department of Electrical Engineering, National Taiwan University, where he is currently a Professor. His research interests include wave propagation, scattering, inverse scattering, and optoelectronics.

Chih-Wei Lu, photograph and biography not available at the time of publication.

I.-Jen Hsu, photograph and biography not available at the time of publication.

Chii-Wann Lin, photograph and biography not available at the time of publication.